Label-free microarray imaging for direct detection of DNA hybridization and single-nucleotide mismatches

Emre Özkumur[a], Sunmin Ahn[b], Ayça Yalçın[a], Carlos A. Lopez[a], Elif Çevik[a], Rostem J. Irani[c], Charles DeLisi[c], Marcella Chiari[d], M. Selim Ünlü[a,*]

[a] Department of Electrical & Computer Engineering, Boston University, Boston, MA, USA
[b] Department of Biomedical Engineering, Boston University, Boston, MA, USA
[c] Center for Advanced Genomic Technology, Boston University, Boston, MA, USA
[d] Istituto di Chimica del Riconoscimento Molecolare (ICRM), C.N.R., Milano, Italy

ABSTRACT

A novel method is proposed for direct detection of DNA hybridization on microarrays. Optical interferometry is used for label-free sensing of biomolecular accumulation on glass surfaces, enabling dynamic detection of interactions. Capabilities of the presented method are demonstrated by high-throughput sensing of solid-phase hybridization of oligonucleotides. Hybridization of surface immobilized probes with 20 base pair-long target oligonucleotides was detected by comparing the label-free microarray images taken before and after hybridization. Through dynamic data acquisition during denaturation by washing the sample with low ionic concentration buffer, melting of duplexes with a single-nucleotide mismatch was distinguished from perfectly matching duplexes with high confidence interval (>97%). The presented technique is simple, robust, and accurate, and eliminates the need of using labels or secondary reagents to monitor the oligonucleotide hybridization.

© 2010 Elsevier B.V. All rights reserved.

1. Introduction

DNA microarray technology is a powerful and versatile tool that is highly utilized in various fields of biology and medicine. The success of DNA microarrays stems from their capability of massive data generation and specific binding detection attributed to Watson–Crick base pairing. The impact of high-throughput platforms has been demonstrated by the utilization of DNA microarrays for many important applications including expression profiling and cancer research (Eisen et al., 1998; Golub et al., 1999; Schena et al., 1995; Wang, 2000). Microarrays are also gaining popularity in medical diagnostics as variations in the DNA sequences of individuals may affect how they develop diseases and respond to treatments (van't Veer et al., 2002). These variations are often observed as differences in a single nucleotide, or single nucleotide polymorphisms (SNP), and SNP detection is being utilized for diagnostic purposes such as evaluating an individual's risk for a certain disease and for genetic analysis in drug discovery (Galbiati et al., 2007; Syvanen, 2001). In order to take advantage of the microarray technology in SNP studies, it is imperative that the technology be capable of resolving single mismatched hybrids

from perfect hybrids which have different binding energies. With conventional fluorescence based detection methods, it is often difficult to relate microarray fluorescence intensity to binding energies (Fish et al., 2007a,b). Thus, complicated procedures are required to accurately quantify the genetic expression levels based on fluorescence detection. As a result, the reliability and the reproducibility of the microarray data are questioned and significant effort is needed to achieve repeatable results such as maintaining uniform and consistent probe coverage for every spotted sample (Draghici et al., 2006; Ramdas et al., 2001; Stears et al., 2003).

Compared to fluorescence detection, label-free detection techniques offer quantitative measurement of interactions and eliminate the necessity of fluorescent labeling (Cooper, 2003; Ramachandran et al., 2005). We have recently introduced a label-free microarray imaging technique, spectral reflectance imaging biosensor (SRIB), which is amenable to high-throughput and dynamic detection of biomolecular interactions on glass surfaces (Ozkumur et al., 2008). SRIB measures the change in optical thickness of a biolayer as a result of mass accumulation and provides quantitative information about the interactions between analytes and immobilized probes (Fig. S1 of supporting information). In this study, we show that the SRIB system can specifically and quantitatively detect the hybridization of surface immobilized oligonucleotides with a target oligonucleotide. Single mismatch discrimination is also demonstrated by successfully distinguishing

a perfectly matched duplex from a duplex containing a mismatch for only one base pair through the study of their denaturation kinetics. Presented technique reveals a very simple and accurate method for high-throughput oligonucleotide sensing and SNP studies.

2. Materials and methods

2.1. SRIB system and detection

Working principles of SRIB were explained elsewhere (Ozkumur et al., 2008). Shortly, a layered substrate of ~17 μm thermally grown SiO$_2$ on Si is used as the solid support for biomolecules and the illumination light goes through multiple reflections from the top surface and SiO$_2$–Si interface which creates an interference signature. The interference signature is characterized by illuminating the surface with a tunable laser and recording intensity images at different wavelengths by a CCD camera, forming a hyperspectral data cube. Part of the laser beam is directed to a single-cell photodetector through a fiber coupler to correct for random intensity fluctuations of the laser light (Fig. S2) (Ozkumur et al., 2009). Hyperspectral data is processed to find the total optical thickness between the reflecting interfaces for the whole surface in the field of view. The biolayer thickness of each spot is found using a custom software which calculates the average optical thickness included in a circle (oxide + biomaterial) and subtracts the average optical thickness included in an annulus surrounding this circle (oxide only) (Fig. S3).

Silicon wafers (Silicon-Valley Microelectronics), the tunable laser (NewFocus—TLB6300), the CCD camera (Q-Imaging—Rolera-XR), and the photodetector (Thorlabs—PDA65) were purchased from various vendors. Instruments were controlled by Labview (National Instruments) during data acquisition, and the data processing was done in Matlab (Mathworks) using custom-built algorithms.

2.2. Surface functionalization

A recently introduced surface functionalization technique was used to coat the silicon substrates prior to oligonucleotide spotting. This method is explained in detail elsewhere (Cretich et al., 2004; Pirri et al., 2004). Shortly, as the first step, the polymer copoly(N,N-dimethylacrylamide (DMA)–acryloyloxysuccinimide (NAS)–3(trimethoxysilyl)-propyl methacrylate (MAPS)) is synthesized. In the second step, clean SiO$_2$ surfaces are treated for 30 min with 0.1 M NaOH for the introduction of OH$^-$ groups on the surface, and washed in DI water for 10 min. The chips are then immersed in the polymer solution (1%, w/v polymer in a water solution of ammonium sulfate at a 20% saturation level) for 30 min, washed extensively with DI water, dried with argon, and baked in the 80 °C oven for 15 min. The polymer-coated chips are kept in the dessicator until use. The copoly(DMA–NAS–MAPS) prepared this way self-adsorbs to the surface and enables covalent attachment of amino-modified oligonucleotides.

2.3. Oligonucleotide probe design

All DNA sequences were purchased from Integrated DNA Technologies (IDT). The sequences of all the oligonucleotides used in this study are shown in Table 1. The oligonucleotides were designed to have minimum self-complementary interaction and approximately equal AT and GC content. The C–C mismatch was introduced in the middle of the sequence in case of the single mismatch probes and every third of the sequence in the case of the double mismatch probes to maximize duplex instability (Peyret et al., 1999). Thermodynamic parameters for the sequences were confirmed with the

Oligo Analyzer provided by IDT. All probes were amino modified at the 5′ end to enable their covalent attachment to the polymer coating on the surface. One 20-mer target sequence was used. One base from each end of the 20-mer probe sequences was excluded for the 18-mer probes. 40-mer probe (40(−)) with no complementary region to the target was used as the negative control. Double stranded 20-mer (20ds), which was hybridized in solution prior to spotting, was also used as an additional control. Hybridization of the duplex was carried out with equimolar amounts of the 20-mer perfect match strands and the target strands in 2× SSC by heating the sample to 85 °C for 3 min and letting it cool slowly to room temperature.

2.4. Spotting and hybridization

Substrates with 17 μm oxide were used for spotting following the surface functionalization. All probes were spotted at 25 μM concentration in 150 mM potassium phosphate buffer (pH 8.5) with BioOdyssey™ Calligrapher™ MiniArrayer (Bio-Rad). The spotted arrays were left in a humid chamber overnight and washed the next day. The washing procedure consisted of four 10-min washes with 6× SSPE containing 0.01% Tween-20 at 40 °C with agitation. The arrays were dried with argon gas and scanned with SRIB, and/or stored in a dessicator for later use.

The spotted arrays were incubated with the hybridization solution containing 1 μM target DNA for 2 h at 40 °C. The hybridization buffer was composed of 100 mM MES, 1 M [Na$^+$], 20 mM EDTA and 0.01% Tween-20. At the end of the hybridization, the sample was washed with the same protocol that was used after spotting, then dried with argon gas for scanning.

3. Results

3.1. End-point detection of DNA hybridization

The DNA samples listed in Table 1 were spotted on a substrate that was functionalized with a novel polymeric coating developed for conventional glass microarray slides (Cretich et al., 2004; Pirri et al., 2004). It has been shown that this surface coating provides high functional probe density by significantly increasing its volume when immersed in buffer (Yalcin et al., 2009). Since the SRIB utilizes a SiO$_2$ surface for probe immobilization, the coating was readily applied.

The complete array was formed of 4 replicate arrays, containing a total of 40 replicate spots for each DNA sample (Fig. 1a). The spots are labeled according to their strand length (20 for 20-mers and 18 for 18-mers), and how they match the target sequence (PM for perfect match, MM for single mismatch, and DM for double mismatch). The sequence labeled as 40(−) is a random sequence used for the negative control. The 20ds sequence is a double-stranded oligonucleotide sequence formed by hybridizing the 20PM sequence with the target strand in solution, prior to spotting.

After probe immobilization and washing, the sample was scanned with SRIB and the biolayer thickness for each spot was found and visualized in a gray-scale image (Fig. 1a). After hybridization, the sample was scanned again, and the initial data was subtracted from the post-hybridization data to find the incremental mass changes on the spots (Fig. 1b). The specific binding of the target to the 20-mer and 18-mer single strands is clearly seen whereas there is no binding to the 40(−) and the 20ds. The faint spot outlines for 40(−) and the 20ds are seen in the difference image, Fig. 1b, because of the registration error between the pre-hybridization (Fig. 1a) and post-hybridization (data not shown) images. Reduced hybridization for the double mismatched spots of 20DM and 18DM are visible as weaker spot intensities in the difference image.

Table 1
The DNA sequences used in the experiments.

Name	Sequence specifics	Sequence
Target	20-mer target	5′/TGC AGA CGA CCA GCG GAA AT/3′
20PM	20-mer, 5′ amine; complement to target	5′/ATT TCC GCT GGT CGT CTG CA/3′
20MM	20-mer, 5′ amine; 1 mismatch (underlined) introduced	5′/ATT TCC GCT CGT CGT CTG CA/3′
20DM	20-mer, 5′ amine; 2 mismatches (underlined) introduced	5′/ATT TCC CCT GGT CCT CTG CA/3′
18PM	18-mer, 5′ amine; complement to target	5′/TTT CCG CTG GTC GTC TGC/3′
18MM	18-mer, 5′ amine; 1 mismatch (underlined) introduced	5′/TTT CCG CTC GTC GTC TGC/3′
18DM	18-mer, 5′ amine; 2 mismatches (underlined) introduced	5′/TTT CCC CTG GTC CTC TGC/3′
40(−)	40-mer, 5′ amine	5′/CGA CGA CCG GAA ACT TTT ATA GCG CAA AAA AAA AAA A/3′
20ds	20-mer duplex of 20PM, 5′ amine; and target	5′/ATT TCC GCT GGT CGT CTG CA/3′
		3′/TAA AGG CGA CCA GCA GAC GT/5′

The mass density of each spot was measured for each image using the annuli method described briefly in Section 2.1 (Ozkumur et al., 2008). SRIB measures the optical thickness of biolayers, and the average film thicknesses are found for each spot assuming a constant refractive index of 1.46. For the conversion of film thickness to biomass density on the surface, the conversion rate of 1 nm corresponding to ~0.8 ng/mm^2 is used, which has been recently determined for ssDNA through careful calibration experiments (Ozkumur et al., 2009). Normalization is applied to the measured mass densities to correct for the refractive index difference between ssDNA and dsDNA. It is known that the refractive index for DNA shifts from ~1.46 (ss) to ~1.54 (ds) upon hybridization and therefore the mass increase upon hybridization was normalized accordingly (Elhadj et al., 2004).

Initial and final spot mass densities are shown in Fig. 1c, and the hybridization efficiencies are calculated using the average incremental mass increases and plotted in Fig. 1d. Although end-point detection was accurate enough to distinguish double mismatches from the perfect match, single mismatches did not show a difference that is as easily distinguishable. Kinetic denaturation experiments were conducted to measure the differences in duplex stabilities, and thus, discriminate the single mismatch from the perfect match.
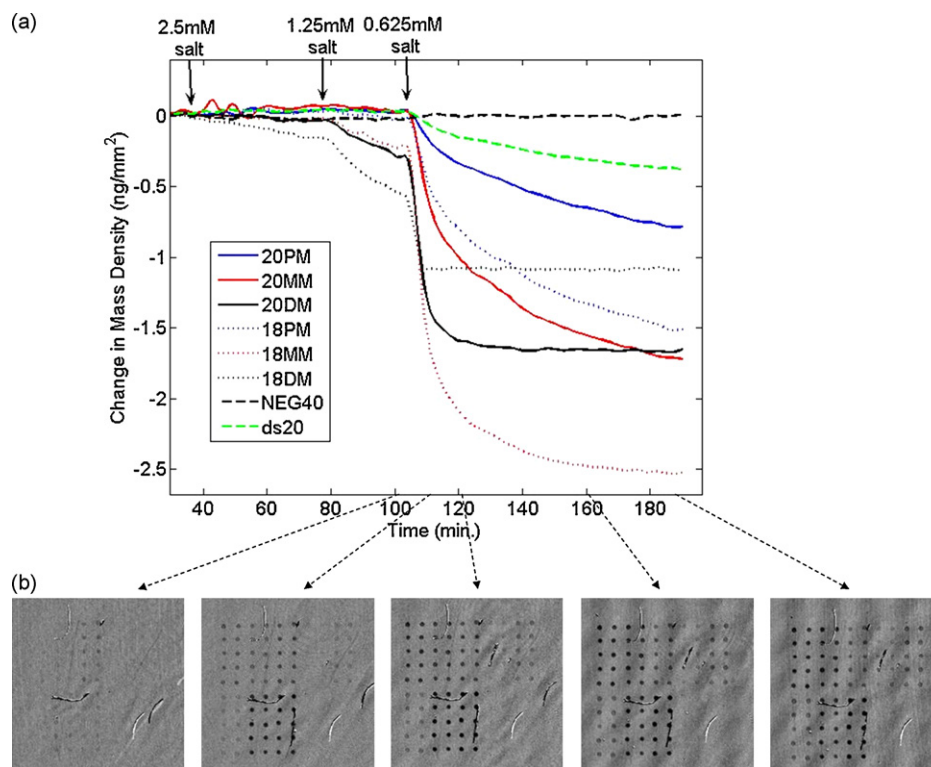
3.2. Ionic concentration dependent denaturation

The slide with DNA spots that was hybridized as described in the previous section was placed in a flow-chamber for kinetic measurements of denaturation. Initially, a high salt (1 M) buffer was used to wash the flow-chamber, flow elements and the sample. During data acquisition, the salt concentration of the wash buffer was gradually lowered at indicated time points as shown in Fig. 2. As the ionic concentration of the buffer is decreased, the shielding of the charges on the negatively charged DNA backbone is reduced, therefore decreasing the stability of the duplex and causing denaturing. This is detected as a drop in the mass densities of the spots (Fig. 2).

During data acquisition, the slide was first incubated with 1 mM MES containing 10 mM [Na$^+$] and 0.01% Tween-20, for 20 min at room temperature. The solution was then diluted 1:1 with deionized (DI) water, bringing the salt concentration down to 5 mM, and no mass change was seen for ~20 min. The salt concentration
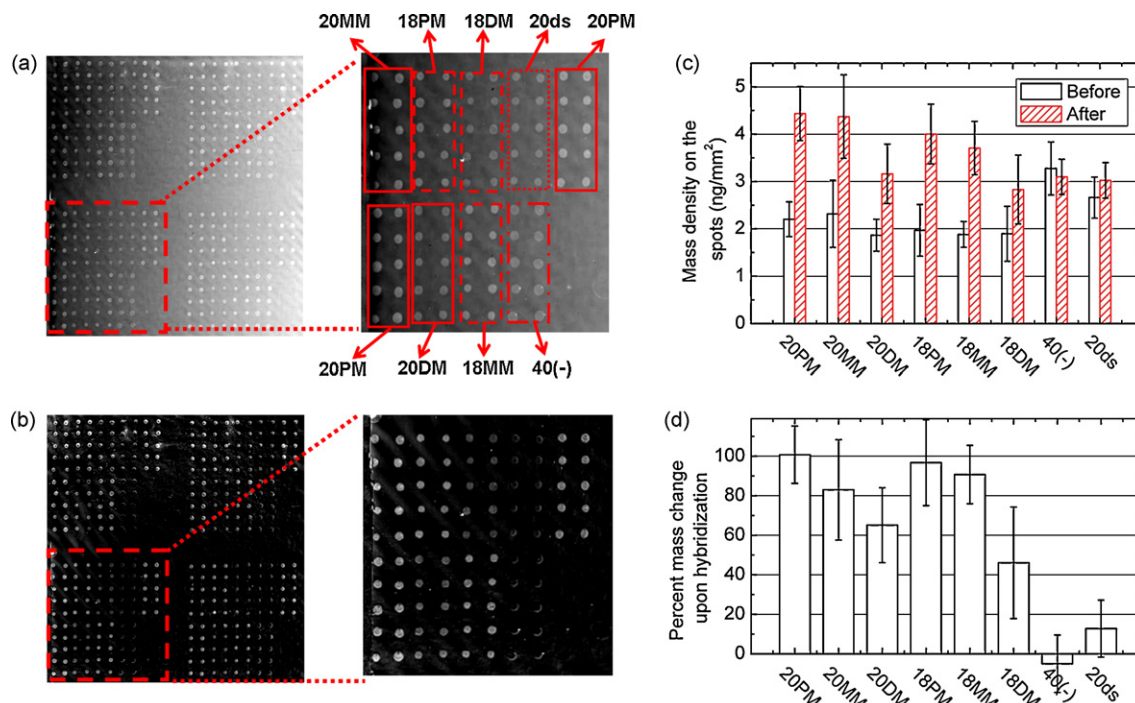
Fig. 1. End-point DNA hybridization detection. (a) The original image of the array is seen after washing the spotted substrate. The 360-spot array contains 4 replicate arrays; in each array, every DNA sample was spotted as 10 replicates. (b) The difference image after hybridization clearly shows mass increase on the specific spots and no hybridization on the control spots of 40(−) and 20ds. (c) Average mass densities on the spots measured before and after hybridization for different DNA strands are shown (n = 40). Error bars represent ±1 standard deviation of measured mass densities among the spots. (d) Percent mass change as a result of hybridization. Error bars represent ±1 standard deviation of detected mass change among the replicate spots. For the perfectly matched duplexes, hybridization is clearly detected and the efficiency is close to 100%.

Fig. 2. The dependence of DNA denaturation kinetics on ionic buffer concentration. (a) 30 spots per probe type are averaged in the denaturation curves. The denaturation of 18DM strands starts when the salt concentration of the buffer is about 2.5 mM, indicating that it is the least stable duplex that is being tested. Incubation with a buffer of 0.625 mM salt concentration initiates denaturation of all duplexes. Notice that the total drop in mass density depends on how much initial hybridization was present, thus, the mismatches cannot be distinguished by the level of mass density drop. However, how fast this drop occurs gives information about duplex stability. (b) The images from the real-time experiment show denaturation patterns of the different duplexes. Since the data at $t = 80$ min is subtracted as a reference, the spots are only visible if there is mass change. The spots begin to darken indicating a decrease in the mass density as denaturation occurs. The images correspond to time points (from left to right): $t = 100$ min; $t = 110$ min; $t = 120$ min; $t = 160$ min; $t = 190$ min.

was reduced to 2.5 mM around the 40th min, where denaturing of 18DM strands was observed. After reducing the ionic concentration further to 1.25 mM, 20DM and 18MM began to dissociate, and the denaturation rate for 18DM increased. Finally, by introducing 0.625 mM salt solution, all the spots that had been hybridized showed a mass decrease indicating denaturation.

The DNA denaturation experiment is summarized in Fig. 2, which shows the differential mass change on the spots averaged for each type of strand. The initial data recorded at the first scan was subtracted from the consecutive data (baseline), thus 0 ng/mm² corresponds to no change in mass density. Notice that the level the mass density drops to is not a good indicator of duplex stability, as it depends on: (1) how many strands were initially immobilized on each spot prior to hybridization; (2) the amount of hybridization achieved at each spot after the target incubation and washing. The denaturation kinetics is a more accurate measure of duplex stability because it depends only on the binding strength of the strands.

3.3. Mismatch detection by measuring denaturation kinetics

In Fig. 3, the kinetic data for 45 spots of 20-mers are shown as a ratio between each spot's mass density changing in time and its initial mass density. Clearly, the fastest mass decrease is seen in 20DM spots, whereas the denaturation of 20PM is slowest, and both the single mismatches and double mismatches are distinguishable from the perfectly matched complementary. To be more accurate with kinetic measurements, the decay rates were found by fitting single exponentials to the kinetic data acquired for each spot, as exemplified in the inset in Fig. 3 for perfect match and single mismatch spots. Only the part of the data after t_1 was used, where all strands started showing noticeable denaturation following the
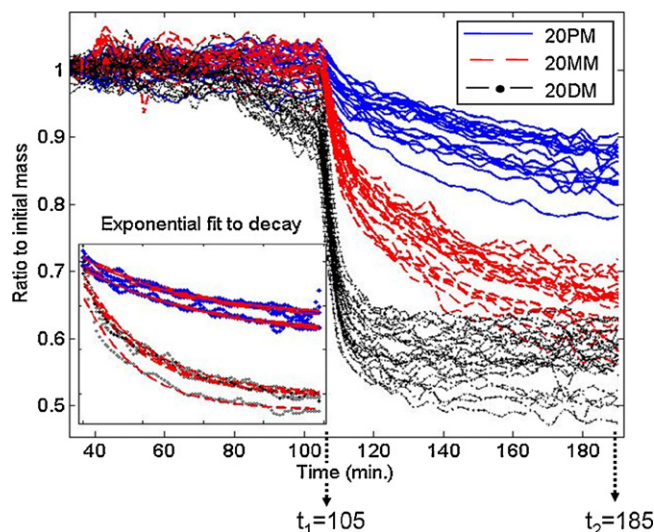
Fig. 3. Kinetic characterization of DNA denaturation. Data for 15 individual spots of 20PM, 20MM and 20DM are shown for demonstration; kinetic data belonging to other samples were processed identically. Single decaying exponentials were fit to each of the denaturation curves for the time period between $t_1 = 105$ min and $t_2 = 185$ min, to find the decay constants. In the inset, example fits of randomly selected 4 spots from 20PM samples and 4 spots from 20MM samples are shown by plotting both their kinetic data and the corresponding fits (shown in red). (For interpretation of the references to color in this figure legend, the reader is referred to the web version of the article.)
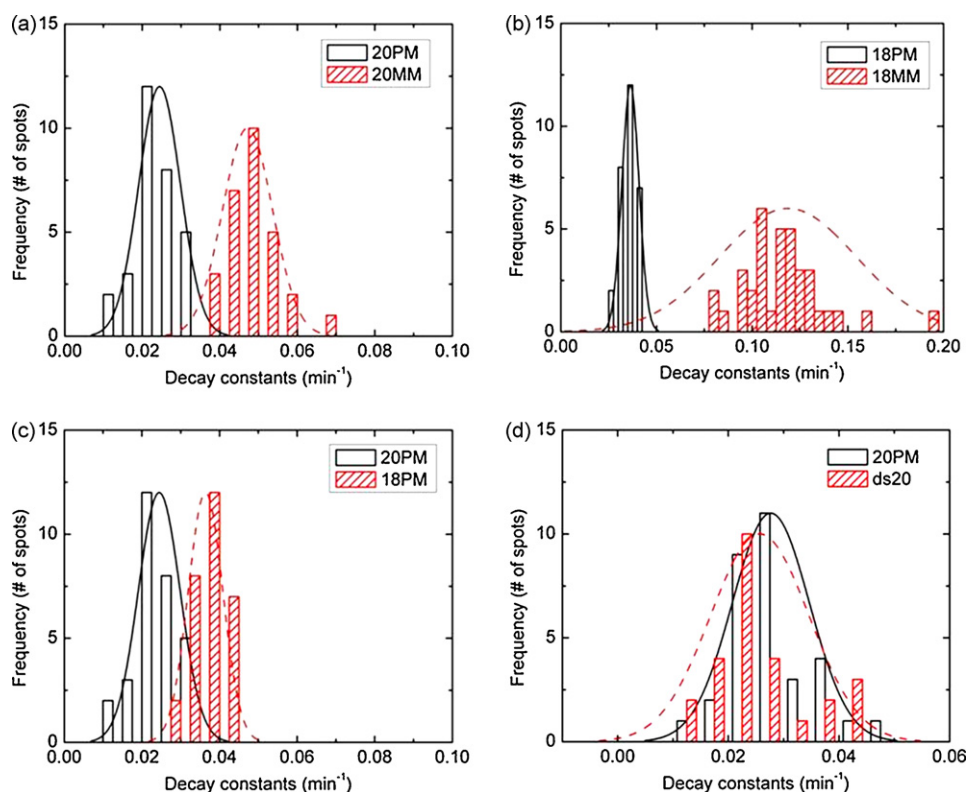
Fig. 4. Denaturation decay constants of DNA duplexes. (a) Decay constants of 20PM and 20MM are compared; (b) decay constants of 18PM and 18MM are compared. A higher decay constant indicates a faster denaturation, thus a less stable DNA duplex. In both cases the single mismatch is clearly detectable. Having a better separation on the 18-nucleotide long sequence indicates a higher impact of the mismatch on the sequence stability. (c) Decay constants of 20PM and 18PM are compared. Even though both of the duplexes were formed by perfectly matching sequences, the shorter strands form slightly less stable duplexes. (d) The similarity of the 20ds and 20PM decay kinetics indicates that the strands that were hybridized prior to spotting and the strands that were hybridized on the chip have the same stability, as expected.

introduction of 0.625 mM salt concentration. The data was characterized with the exponential function of the form: $f = a_1 e^{-a_2 t} + a_3$ where a_1, a_2 and a_3 are fitting parameters and t represents the time interval between t_1 and t_2. Although, a_1 and a_3 do not have an experimental significance, their inclusion in the fitting function improves the quality of the fitting and it is not expected that they affect the values found for the decay constant, a_2, which is the parameter of interest.

The decay constants, a_2, found from the exponential fits are plotted in Fig. 4 as histograms. In Fig. 4a and b, it is shown that 20PM and 18PM are clearly distinguished from 20MM, and 18MM, respectively. Thus, the single mismatch in the complementary strand is detected both for 20- and 18-nucleotide long strands. Also, as shown in Fig. 4c, 20PM and 18PM show a clear difference in their kinetic behavior, indicating that shorter strands form less stable duplexes as expected, and that even these minute changes in the stability of the DNA is detectable with SRIB. The confidence intervals calculated for 20-mer single mismatch detection is 97.2%, for 18-mer single mismatch detection is 98.6%, and for distinguishing 20PM from 18PM is 88.7% (Fig. S4). The confidence intervals

improve above 99% easily by averaging the data belonging to replicate spots. The decay constants found for 20DM and 18DM are 10-fold higher than those of PM and MM spots and they are left out of the plots for clarity. Table 2 summarizes the decay constants for all of the duplexes. Finally, the 20PM and 20ds strands do not have a noticeable difference in their kinetic denaturation rates as shown in Fig. 4d, indicating that 20 nucleotide long duplexes that were hybridized prior to spotting have the same stability as the strands that were hybridized on the surface.

4. Discussion

An important requirement of the DNA sensing platforms is the ability to distinguish single-nucleotide mismatches for SNP studies. A common method for genotyping SNPs uses MALDI-TOF MS (matrix assisted laser desorption/ionization time of flight mass spectrometry). Mass spectrometry has the label-free capability. However, in order to increase resolution, samples are usually labeled with mass tags during primer extension or amplification prior to most MALDI-TOF MS based detection methods for SNP

Table 2
Denaturation decay constants.

	20PM	20MM	20DM	18PM	18MM	18DM
Mean	2.47×10^{-2}	4.72×10^{-2}	23.0×10^{-2}	3.64×10^{-2}	11.8×10^{-2}	51.2×10^{-2}
Standard deviation	0.54×10^{-2}	0.65×10^{-2}	3.93×10^{-2}	0.45×10^{-2}	3.59×10^{-2}	15.0×10^{-2}
CI (%)[a]	–	97.2%	100%	–	98.6%	100%
ΔG [b] (kcal/mol)	−34.2	−28.3	−21.2	−32	−26.1	−18.9

[a] Confidence interval describes the confidence in identifying specie from its corresponding perfectly complementary duplex. Calculation is described in the supplementary material (Fig. S4).

[b] ΔG was calculated with the DINAMelt Server (http://dinamelt.bioinfo.rpi.eu). The parameter used for the calculation is as follows: 20 °C hybridization temperature, 900 mM [Na], 1 μM target concentration.

genotyping (Fei et al., 1998). Mass spectrometry generally performs with limited throughput but there are efforts to increase this throughput (Ding and Cantor, 2003). However, these systems can be very expensive and bulky, and their utilization requires careful sample preparation. Also, fragmentation of samples can cause major inaccuracies in the acquired data (Tang et al., 1997).

Some SNP genotyping solutions that are commercially available offer high-throughput detection through utilization of microarrays (Nicolae et al., 2006; Shen et al., 2005). However, differences in surface functionalization, spotting and labeling techniques, and variations in experimental protocols may cause poor reproducibility of data in microarray platforms. Varying surface immobilization efficiencies affect the total fluorescence signal. Since the initial densities of probe molecules cannot be measured with labeled detection methods, the quantification of hybridization reactions is quite complicated. Also, knowing the probe densities is crucial for correct determination of hybridization dynamics as it was shown to affect the thermodynamic kinetics of hybridization reactions (Peterson et al., 2001). Inherent properties of fluorescent labeling may create further errors; Niu and Saraf (2002) have shown that variations in labeling efficiencies produce inaccuracies in the final data, whereas Ramdas et al. (2001) have demonstrated that one of the sources of nonlinearity in DNA arrays is the quenching of fluorophores. These drawbacks limit the user confidence to experimental data and applicability of the technique to clinical diagnostics, and drive the need for label-free detection of DNA. Additionally, eliminating the labeling step would be time and cost efficient.

The development of simple, sensitive, specific, quantitative, and high-throughput sensors is an area of increasing interest. Techniques that utilize foerster resonance energy transfer (FRET) were recently developed to detect the hybridization of molecular beacons with non-labeled target strands (Du et al., 2005; Marras et al., 1999; Tyagi and Kramer, 1996; Wang et al., 2002; Yao and Tan, 2004). Nanoparticle attached secondary probes (Taton et al., 2000) have also shown to improve the sensitivity and selectivity of DNA detection. These methods are not direct measurements of the hybridization and utilize secondary reagents or fluorescent signal to quantify the captured target. Thus spot-to-spot surface uniformity or accurate calibration of the signal is required for quantitative detection. Electrochemical DNA sensors (Drummond et al., 2003; Kelley et al., 1999; Weng et al., 2008), carbon nanotube (CNT) electrode arrays (Koehne et al., 2003, 2004), and nanowire sensors (Hahm and Lieber, 2004) have shown highly sensitive DNA detection capabilities, but individually addressing each sensor presents a significant challenge toward highly multiplexed detection. Furthermore, these techniques are often highly complex.

Recently, optical label-free detection methods have gained significant popularity for applications that require kinetic characterization of biomolecular interactions (Cooper, 2002; Mitchell, 2002; Ramachandran et al., 2005). Even though label-free biosensors are commonly used for protein arrays, their utilization for DNA microarrays has been rather limited; one of the reasons being decreased sensitivity due to low molecular weight of short nucleic acid sequences. SRIB has proven to be a powerful tool for label-free microarray imaging, and it has been shown that quantitative interaction kinetics can be measured with this technique (Ozkumur et al., 2008).

In this paper, we demonstrate that the SRIB system is capable of detecting hybridization reactions in a very simple configuration. Hybridization of ssDNA is clearly detectable by comparing the mass density of the spots prior to and after hybridization. Although the signal of hybridization is well above the noise floor, the level of mass increase upon hybridization or mass decrease upon denaturation are not ideal ways of distinguishing the perfect match from mismatches. However, as shown with the dynamic measurements,

the kinetics of the denaturation is clearly different for perfect complement and mismatch strands. Here, we make use of the difference in denaturation kinetics as an indication of the duplex stability and utilize it for the detection of single mismatches. Only the dependence of the duplex stability to ionic concentration of washing buffer is tested in the presented work, but temperature dependent denaturation characteristics can be measured with sophisticated flow-chambers. Naturally, the hybridization kinetics of perfect and mismatched hybrids is expected to be different, as well. However, the ionic concentration and temperature of the hybridization buffer should be carefully adjusted to successfully resolve the difference in hybridization kinetics. It was shown that finding an optimal condition to discriminate a single nucleotide mutation by observing hybridization kinetics can be very difficult in a multiplexed measurement (Fish et al., 2007a,b). Instead, the method proposed in this paper is extremely simple as all strands are hybridized in high salt solution, then the ionic strength of wash buffer is reduced gradually during real-time data acquisition until the denaturation is detected on all hybrids. Thus, the wash buffer conditions are set in real-time, while monitoring the outcomes. This method gives 88.7% confidence interval for distinguishing the stability of hybrids that have 2.2 kcal/mol difference in their free energy (20PM and 18PM), and the mass sensitivity of the current system is measured as $\sim$0.01 ng/mm^2.

5. Conclusions

The experiments shown in this paper indicate that the SRIB detection system can be utilized for expression analysis and SNP detection. Simultaneous detection of 360 individual spots were shown in this work, however the throughput can be extended to $\sim$10^4 if needed (Ozkumur et al., 2008). The sensing method uses a glass surface, therefore well developed glass chemistries by the microarray community can be used for surface functionalization. Also, the system response is not affected by changes in the temperature or the refractive index of the solution, which permits melting experiments or buffer dependent hybridization and denaturation tests to be conducted. We envision that the SRIB system can be a prominent tool for DNA–DNA studies with a throughput of >10^4 which demand high data accuracy and simplicity.

Acknowledgements

Appendix A. Supplementary data

Supplementary data associated with this article can be found, in the online version, at doi:10.1016/j.bios.2009.12.032.

References

Cooper, M.A., 2002. Nature Reviews Drug Discovery 1 (7), 515–528.
Cooper, M.A., 2003. Analytical and Bioanalytical Chemistry 377 (5), 834–842.
Cretich, M., Pirri, G., Damin, F., Solinas, I., Chiari, M., 2004. Analytical Biochemistry 332 (1), 67–74.
Ding, C., Cantor, C.R., 2003. Proceedings of the National Academy of Sciences of the United States of America 100, 3059–3064.
Draghici, S., Khatri, P., Eklund, A.C., Szallasi, Z., 2006. Trends in Genetics 22 (2), 101–109.
Drummond, T.G., Hill, M.G., Barton, J.K., 2003. Nature Biotechnology 21 (10), 1192–1199.
Du, H., Strohsahl, C.M., Camera, J., Miller, B.L., Krauss, T.D., 2005. Journal of the American Chemical Society 127 (21), 7932–7940.

Eisen, M.B., Spellman, P.T., Brown, P.O., Botstein, D., 1998. Proceedings of the National Academy of Sciences of the United States of America 95 (25), 14863–14868.

Elhadj, S., Singh, G., Saraf, R.F., 2004. Langmuir 20 (13), 5539–5543.

Fei, Z.D., Ono, T., Smith, L.M., 1998. Nucleic Acids Research 26, 2827–2828.

Fish, D.J., Horne, M.T., Brewood, G.P., Goodarzi, J.P., Alemayehu, S., Bhandiwad, A., et al., 2007a. Nucleic Acids Research 35 (21), 7197–7208.

Fish, D.J., Horne, M., Searles, T., Brewood, R.P., Benight, A.S., 2007b. Biophysical Journal 92, L89–L91.

Galbiati, S., Chiari, M., Macellari, M., Ferrari, M., Cremonesi, L., Cretich, M., 2007. Electrophoresis 28 (23), 4289–4294.

Golub, T.R., Slonim, D.K., Tamayo, P., Huard, C., Gaasenbeek, M., Mesirov, J.P., et al., 1999. Science 286 (5439), 531–537.

Hahm, J., Lieber, C.M., 2004. Nano Letters 4 (1), 51–54.

Kelley, S.O., Boon, E.M., Barton, J.K., Jackson, N.M., Hill, M.G., 1999. Nucleic Acids Research 27 (24), 4830–4837.

Koehne, J., Chen, H., Li, J., Cassell, A.M., Ye, Q., Ng, H.T., et al., 2003. Nanotechnology 14 (12), PII S0957-4484(0903)66806-66806.

Koehne, J.E., Chen, H., Cassell, A.M., Yi, Q., Han, J., Meyyappan, M., et al., 2004. Clinical Chemistry 50 (10), 1886–1893.

Marras, S.A.E., Kramer, F.R., Tyagi, S., 1999. Genetic Analysis: Biomolecular Engineering 14 (5–6), 151–156.

Mitchell, P., 2002. Nature Biotechnology 20 (3), 225–229.

Nicolae, D.L., Wen, X., Voight, B.F., Cox, N.J., 2006. PLoS Genetics 2 (5), e67.

Niu, S.J., Saraf, R.F., 2002. Smart Materials & Structures 11 (5), PII S0964-1726(0902)52682-52683.

Ozkumur, E., Needham, J.W., Bergstein, D.A., Gonzalez, R., Cabodi, M., Gershoni, J.M., et al., 2008. Proceedings of the National Academy of Sciences of the United States of America 105 (23), 7988–7992.

Ozkumur, E., Yalcin, A., Cretich, M., Lopez, C.A., Bergstein, D.A., Goldberg, B.B., et al., 2009. Biosensors and Bioelectronics 25 (1), 167–172.

Peterson, A.W., Heaton, R.J., Georgiadis, R.M., 2001. Nucleic Acids Research 29 (24), 5163–5168.

Peyret, N., Seneviratne, P.A., Allawi, H.T., SantaLucia, J., 1999. Biochemistry 38, 3468–3477.

Pirri, G., Damin, F., Chiari, M., Bontempi, E., Depero, L.E., 2004. Analytical Chemistry 76 (5), 1352–1358.

Ramachandran, N., Larson, D.N., Stark, P.R.H., Hainsworth, E., LaBaer, J., 2005. FEBS Journal 272 (21), 5412–5425.

Ramdas, L., Coombes, K.R., Baggerly, K., Abruzzo, L., Highsmith, W.E., Krogmann, T., et al., 2001. Genome Biology 2 (11), RESEARCH0047.

Schena, M., Shalon, D., Davis, R.W., Brown, P.O., 1995. Science 270 (5235), 467–470.

Shen, R., Fan, J.B., Campbell, D., Chang, W., Chen, J., Doucet, D., et al., 2005. Mutation Research 573, 70–82.

Stears, R.L., Martinsky, T., Schena, M., 2003. Nature Medicine 9 (1), 140–145.

Syvanen, A.C., 2001. Nature Reviews Genetics 2 (12), 930–942.

Tang, W., Zhu, L., Smith, L.M., 1997. Analytical Chemistry 69, 302–312.

Taton, T.A., Mirkin, C.A., Letsinger, R.L., 2000. Science 289 (5485), 1757–1760.

Tyagi, S., Kramer, F.R., 1996. Nature Biotechnology 14 (3), 303–308.

van't Veer, L.J., Dai, H.Y., van de Vijver, M.J., He, Y.D.D., Hart, A.A.M., Mao, M., et al., 2002. Nature 415 (6871), 530–536.

Wang, H., Li, J., Liu, H.P., Liu, Q.J., Mei, Q., Wang, Y.J., et al., 2002. Nucleic Acids Research 30 (12).

Wang, J., 2000. Nucleic Acids Research 28 (16), 3011–3016.

Weng, J., Zhang, J.F., Li, H., Sun, L.P., Lin, C.H., Zhang, Q.Q., 2008. Analytical Chemistry 80 (18), 7075–7083.

Yalcin, A., Damin, F., Ozkumur, E., di Carlo, G., Goldberg, B.B., Chiari, M., et al., 2009. Analytical Chemistry 81 (2), 625–630.

Yao, G., Tan, W.H., 2004. Analytical Biochemistry 331 (2), 216–223.